NANO · MICRO small
www.small-journal.com

Targeted Delivery of Sucrose-Coated Nanocarriers with Chemical Cargoes to the Plant Vasculature Enhances Long-Distance Translocation

*Su-Ji Jeon, Yilin Zhang, Christopher Castillo, Valeria Nava, Kurt Ristroph, Benjamin Therrien, Leticia Meza, Gregory V. Lowry, and Juan Pablo Giraldo**

Current practices for delivering agrochemicals are inefficient, with only a fraction reaching the intended targets in plants. The surfaces of nanocarriers are functionalized with sucrose, enabling rapid and efficient foliar delivery into the plant phloem, a vascular tissue that transports sugars, signaling molecules, and agrochemicals through the whole plant. The chemical affinity of sucrose molecules to sugar membrane transporters on the phloem cells enhances the uptake of sucrose-coated quantum dots (sucQD) and biocompatible carbon dots with β-cyclodextrin molecular baskets (suc-β-CD) that can carry a wide range of agrochemicals. The QD and CD fluorescence emission properties allowed detection and monitoring of rapid translocation (<40 min) in the vasculature of wheat leaves by confocal and epifluorescence microscopy. The suc-β-CDs more than doubled the delivery of chemical cargoes into the leaf vascular tissue. Inductively coupled plasma mass spectrometry (ICP-MS) analysis showed that the fraction of sucQDs loaded into the phloem and transported to roots is over 6.8 times higher than unmodified QDs. The sucrose coating of nanoparticles approach enables unprecedented targeted delivery to roots with ≈70% of phloem-loaded nanoparticles delivered to roots. The use of plant biorecognition molecules mediated delivery provides an efficient approach for guiding nanocarriers containing agrochemicals to the plant vasculature and whole plants.

1. Introduction

The increasing global demand for agricultural productivity by a rapidly growing population requires a large increase in food production.[1,2] Agricultural practices wield some of the earth's most significant pressures on natural resources, leading to deforestation, groundwater pollution, and increased greenhouse gas emissions.[3,4] The large inefficiencies of agrochemical delivery for pesticides and fertilizers in agricultural land are among the most negative impacts on environmental and human health.[5] Pesticides such as insecticides, fungicides, and herbicides a major class of agrochemicals, accumulate in the environment, and through biomagnification can move into the food chain or affect non-target species.[6,7] While pesticides increase crop yield and quality, frequent use leads to resistance to agricultural pests (i.e., pathogens and weeds), impacts air quality and contaminates water and soil.[8–10] Pesticide usage is particularly concerning since only a small fraction[11] of millions of metric tons of these agrochemicals applied annually worldwide[12–14] reach the intended biological target. Herbicides lacking systemic translocation across whole plants also impair their effectiveness in combating weeds requiring larger frequency and amount of application in crop fields.[15] A solution toward these inefficiencies is rooted in the ability to precisely deliver the agrochemicals to their intended targets in plants where and when they will be most effective. To achieve this, new technologies and delivery approaches are needed to increase the efficiency of agrochemical delivery.[2,16]

Over the past decade, nanotechnologies have emerged as tools to meet agricultural demands and offer potential solutions to mitigate the inefficiencies of agrochemical delivery.[17,18] Seminal studies demonstrating the ability of nanomaterials to bypass plant cell barriers led to a growing interest in using them as tools for the delivery of chemical and biomolecule cargoes in plants.[19] The tunable physical and chemical properties of nanomaterials enable a higher delivery efficiency to specific targets in plants. For example, the size and charge of nanomaterials can influence their foliar delivery efficiency to plant cells and organelles, including stomata guard cells and chloroplasts.[20] Targeted and controlled release studies for biomedical applications set a foundation for the field of nano-enabled agriculture to use nanocarriers for improving the delivery of agrochemicals in plants.[21] Recently, we have demonstrated that engineered nanomaterials can be guided

S.-J. Jeon, C. Castillo, L. Meza, J. P. Giraldo
Department of Botany and Plant Sciences
University of California
Riverside, CA 92521, USA
E-mail: juanpablo.giraldo@ucr.edu
Y. Zhang, V. Nava, K. Ristroph, B. Therrien, G. V. Lowry
Department of Civil and Environmental Engineering
Carnegie Mellon University
Pittsburgh, PA 15213, USA

The ORCID identification number(s) for the author(s) of this article can be found under https://doi.org/10.1002/smll.202304588

DOI: 10.1002/smll.202304588

by peptides that target chemical cargoes to plant organelles.[22,23] Plant biorecognition approaches to target nanomaterials to plant-specific cells and organelles have been exploited for delivery to plant stomata, trichomes, and chloroplasts.[22,24] However, a main agricultural need is to target the plant vasculature where the phloem vascular tissue is a primary route for long distance and systemic agrochemical translocation in plants[25–27] and the hosting site of devastating plant pathogens that impair crop yields.[28] Recently, targeted delivery approaches mediated by nanomaterials have focused their attention on the plant phloem.[29]

The plant phloem offers a transport system for agrochemical translocation from leaves to other plant organs, including stems and underground roots, without interacting with complex and diverse types of soil matrices.[30] In contrast, nanoparticle delivery to plants through the roots is limited due to the selective permeability of roots and the presence of various barriers such as the root endodermis which can hinder plant uptake into the vasculature.[31] Long-distance phloem transport of organic compounds such as amino acids and photosynthetic products (i.e., sugars) from leaves to other organs is driven by bulk flow through sieve vascular elements and loading and unloading of phloem sap from cell-to-cell in phloem companion cells.[32–34] Mechanisms for loading molecules into the phloem and translocation to plant organs vary among plant species and have been reported by previous studies.[35] However, approaches for enhancing nanomaterial delivery and loading into phloem tissues have not been elucidated. Oparka and colleagues reported functionalizing molecules with sucrose to induce sucrose transporters and enhance uptake into the phloem through sucrose-uptake transporters.[35] Plant transport of sucrose, a primary sugar transported in the phloem of plants, is highly regulated and requires sucrose transporters.[32,34] These innate mechanisms of sucrose recognition and transport by the phloem provide an untapped opportunity to target nanomaterials with agrochemical cargoes.[36–39] Approaches using the molecular machinery of plants to target nanomaterials to the phloem have not been explored. Current methods for delivering chemicals to the phloem rely on conjugation with antibodies that are inadequate for agricultural applications due to their high costs and stability at ambient conditions.[40–42] Herein, we tested an alternative approach using surface functionalization of nanoparticles with biorecognition molecules of sucrose that can be scalable and low cost. These nanoparticles have a distinct capability to bypass plant cell barriers including the plasma and organelle membranes by passive disruption of lipid bilayers.[43,44]

Quantum dots (QDs) exhibit optical and electronic properties that make them model traceable nanoparticles for assessing interactions with plant biointerfaces using multiple advanced analytical tools.[45,46] The QDs are intrinsically bright and offer non-photobleaching fluorescence with tunable emission wavelength for imaging in plants at high spatial and temporal resolution by confocal fluorescence microscopy.[22] Quantitative analysis of the distribution of QD core elements, such as cadmium and tellurium, can be performed in plant tissues using inductively coupled plasma mass spectrometry (ICP-MS). Furthermore, QD tunable surface chemistry permits coating with biorecognition motifs for targeted delivery to plant tissues, cells, and organelles.[47] Combined, QDs are valuable tools for tracking and quantifying the targeted delivery of nanomaterials in plants for a fundamental understanding of nanoparticle-plant interactions. However, metal-based QDs are not suitable for environmental and agricultural applications as their degradation could release toxic metals into the environment, potentially posing human health and environmental risk.[48] Carbon-based quantum dots (CDs) coated with molecular baskets (β-cyclodextrins) can carry a wide range of agrochemicals[22,49,50] and have been recently demonstrated to act as targeted chemical delivery platforms for plant organelles.[23] CDs are among the most biocompatible and environmentally friendly nanomaterials[51,52] with large potential for nano-enabled agriculture applications.[53–58] Understanding foliar delivery mechanisms of nanomaterials to the plant vasculature is paramount for the adoption of nano-based technologies for scalable, efficient, and systemic agrochemical delivery. Previous studies investigating QD and CD deliveries to the plant phloem have reported the introduction of the nanomaterials with mechanical aid, feeding through excised stems, or addition to the hydroponic growth medium of seedlings.[59–61] Despite these advances, there are no efficient and scalable approaches nor a mechanistic understanding of how to target nanomaterials to the phloem in more realistic conditions in intact live plants grown in soil, thus limiting applications of nanotechnology for agrochemical foliar delivery through the plant vasculature.

This study elucidates how foliar delivery of QD and CD coated with sucrose molecules enables targeted delivery to the phloem and enhances long-distance translocation in wheat plants (*Triticum aestivum*). We hypothesized that delivery of QD and CD with β-cyclodextrins (β-CD) to the phloem is significantly improved by sucrose moieties on the nanoparticle surface that bind to sucrose transporters in phloem sieve membranes followed by uptake into the phloem through the lipid cell membrane (**Figure 1**). We performed confocal and epifluorescence microscopy to determine the nanoparticle distribution in plant leaves and their translocation rates into the leaf phloem, confirmed their loading into the vasculature by synchrotron X-ray fluorescence mapping, and quantified their uptake and long-distance transport from leaves to roots and stems by ICP-MS analysis. We also demonstrated that suc-β-CDs enhance the delivery of fluorescent chemical cargoes into the leaf vasculature. Targeting of traceable CD with molecular baskets to the phloem can act as tools for improving agrochemical delivery technologies and lead to a more precise and sustainable agriculture.

2. Results

2.1. Characterization of Nanoparticles for Targeted Delivery to the Phloem

Sucrose molecules were coated on the QD (sucQD) or β-CD (suc-β-CD) surface by strong binding between boronic acid groups and carbohydrates (i.e., sucrose) containing syn-periplanar hydroxyl groups (Figure S1, Supporting Information).[22] We functionalized the CD with β-cyclodextrin molecular baskets to act as targeted nanocarriers for the delivery of agrochemicals in plants (Figure S1, Supporting Information). β-cyclodextrins have been shown to load and deliver a wide range of chemicals including pesticides and herbicides (Table S1, Supporting Information).[22,49,50] Transmission electron microscopy (TEM) images showed an average size of sucQD and suc-β-CD of

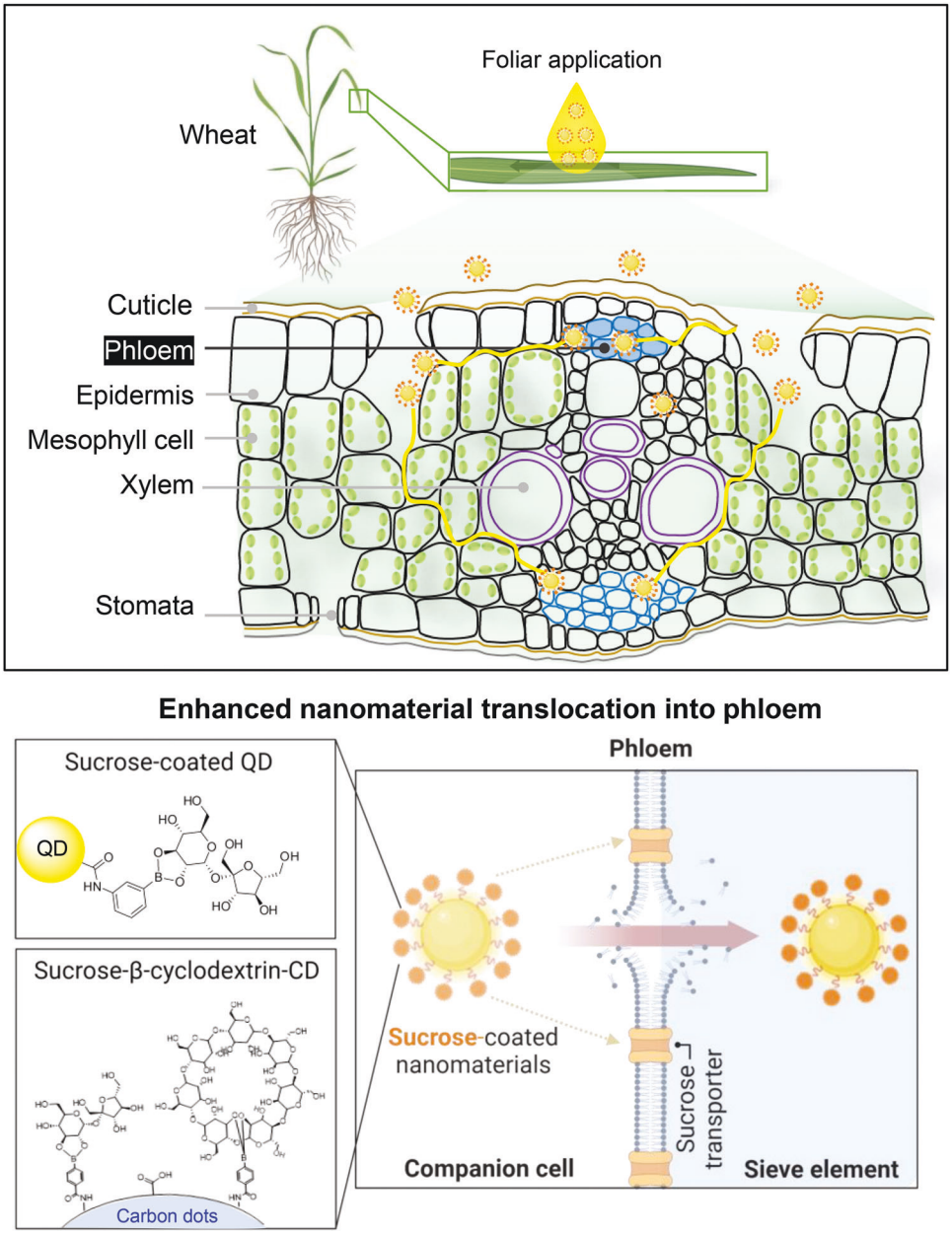

Figure 1. Targeted delivery of sucrose-coated nanomaterials to the phloem. Foliar applied quantum dots (sucQDs) and β−cyclodextrin carbon dots (suc-β−CDs) coated in sucrose are guided through leaf tissues to the plant vasculature via binding with sucrose transporters located in phloem vessels. The nanoparticles bypass leaf cell barriers and penetrate phloem cells through disruption of the lipid membrane, followed by bulk flow transport through the phloem from the leaves to other plant organs.

≈5.0 ± 0.8 and 9.1 ± 2.8 nm, respectively (Figure S2, Supporting Information). The suc-β-CDs were doped with gadolinium (suc-β-GdCDs) for X-ray fluorescence mapping analysis. Gadolinium is incorporated into the core structure of the CDs via coordination bonds during the carbon dot synthesis.[62,63] The hydrodynamic diameter of QD, CD, and GdCD was measured before and after functionalization with sucrose or β-cyclodextrin. The DLS sizes of the core QD, CD, and GdCD were 15.3 ± 1.6, 3.6 ± 1.5, and 7.5 ± 4.1 nm, respectively. After functionalization with sucrose or β-cyclodextrin, the sizes of sucQD, suc-β-CD, and suc-β-GdCD increased to a similar level of 17.6 ± 1.4, 20.3 ± 3.6, and 17.4 ± 5.7 nm, respectively (in 10 mM TES, pH 7.4, n = 3) (**Figure 2**a). The hydrodynamic diameter of sucQD and suc-β-CD were larger than their TEM size due to the attachment of organic molecules such as sucrose and cyclodextrin, or dimer and trimer formation not observed in the TEM. Both QDs and sucQDs are highly negatively charged with ζ potential magnitudes of −57.1 ± 2.5 and −45.9 ± 7.4 mV (10 mM TES, at pH 7.0), respectively (Figure 2b). The core CD and GdCD also have negatively charged zeta potentials of −28.9 ± 7.7 and −12.2 ± 1.9 mV, respectively. Coating the

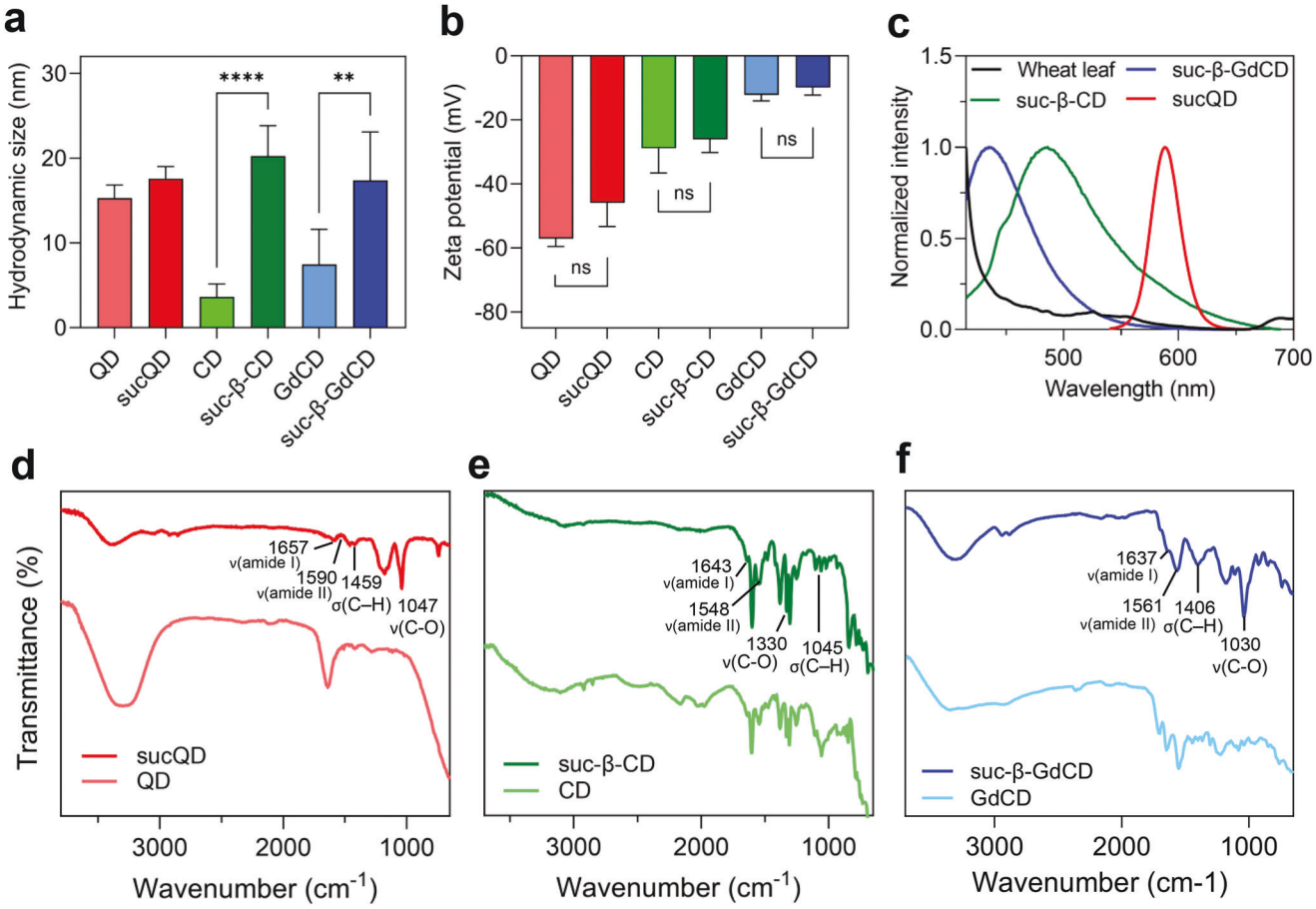

Figure 2. Characterization of quantum dots (QDs) and carbon dots (CDs) for targeted delivery to phloem. a) Hydrodynamic size of QDs, sucQDs, core CDs, and suc-β-CDs, uncoated GdCDs, and suc-β-GdCDs (TES buffer, pH 7.0) ($n = 3$–6). The polydispersity index for all nanoparticles ranges from 0.28 to 0.35. b) zeta potential of QDs, sucQDs, core CDs, and suc-β-CDs, uncoated GdCDs, and suc-β-GdCDs (TES buffer, pH 7.0) ($n = 3$–6). *t*-test (Prism ver. 10, GraphPad), ns (non-significant), ** $p < 0.5$, **** $p < 0.0001$. c) Fluorescence emission spectra of sucQD, suc-β-CD, and suc-β-GdCD. Both sucQD and suc-β-CD fluorescence have minimal overlap with leaf background fluorescence. d–f) FT-IR spectra of sucQDs, suc-β-CDs, and suc-β-GdCD indicate functionalization with sucrose and/or β-cyclodextrins on their surface. Error bars represent SD.

CD or GdCD with sucrose and β-cyclodextrins slightly reduces the zeta potential of suc-β-CD and suc-β-GdCD to -26.1 ± 4.1 and -9.9 ± 2.4 mV (Figure 2b). The size and charge of nanoparticles coated in polymers have been reported to control their distribution in plant cells or organelles.[20,30] However, little is known about how these properties influence the translocation and distribution of nanoparticles coated with biorecognition molecules such as sucrose. The DLS size of nanomaterials in this study is in the range (< 40 nm)[30] reported to allow internalization through leaf biosurface barriers, including the plant cell wall, plasma, and chloroplast membranes. The ζ potential for all nanoparticles except for GdCD and suc-β-GdCD is within the range expected to facilitate uptake through plant lipid membranes (> 20 mV).[43]

Both QDs and CDs functionalized with sucrose or β-cyclodextrin molecules maintained their remarkable optical properties and colloidal stability. Although sucQD exhibited the same characteristic absorption peak as QD at 575 nm, the absorbance of sucQD had a slight increase in the UV range, attributed to the introduction of sucrose molecules on their surface (Figures S3 and S4, Supporting Information). The absorption spectrum of suc-β-CD showed the broadening of CD absorption in the UV and visible range due to the introduction of both sucrose molecules and β-cyclodextrins (Figure S4, Supporting Information). The suc-β-GdCDs also showed both of their characteristic absorption peaks at 355 nm[62,64] and broad absorption in the range of 300 to 450 nm after functionalization (Figure S4, Supporting Information). To determine the colloidal stability of sucQD and suc-β-GdCD in plant vasculature fluid, we measured their absorbance at 575 and 355 nm, respectively, while they were dispersed in artificial phloem sap for 7 days (Figure S5, Supporting Information). The absorbance of sucQD and suc-β-GdCD did not change during this timeframe, confirming their colloidal stability in artificial phloem sap. One of the remarkable properties of QD and CD is their high, tunable, and stable fluorescence that allows tracking of their translocation and distribution within leaf tissues and cells.[20,23] The maximum fluorescence emission peak for sucQD, suc-β-CD, and suc-β-GdCD was 590, 490, and 420 nm, respectively (Figure 2c). The QD and CD fluorescence emission spectra minimize optical interference with autofluorescence from leaves within the

imaging detection range of 450–680 nm (Figure 2c).[20,22] We confirmed the functionalization of QD, CD, and GdCD with sucrose and/or β-cyclodextrins by Fourier transform infrared spectroscopy (FT-IR) (Figure 2d–f). The sucQD, suc-β-CD, and suc-β-GdCD showed characteristic vibrational peaks for: amide I (1657 cm^{-1} for sucQD and 1643 cm^{-1} for suc-β-CD 1637 cm^{-1} for suc-β-GdCD), amide II (1590 cm^{-1} for sucQD and 1548 cm^{-1} for suc-β-CD 1561 cm^{-1} for suc-β-GdCD) due to functionalization with boronic acids through amide bonding; C–H bending of sucrose or β-cyclodextrin molecules (1459, 1413, and 1406 cm^{-1}); B–O stretching from sucQD, suc-β-CD, and suc-β-GdCD (1326, 1330, and 1325 cm^{-1} respectively); C-O stretching of sucrose from all nanoparticles at 1047, 1045, and 1030 cm^{-1}; and C–O or C–O–C stretching of β-cyclodextrin from sucQD, suc-β-CD, and suc-β-GdCD at 1101, 1106, 1108 cm^{-1}, respectively.

2.2. Enhanced Delivery of Sucrose-Coated Nanoparticles to the Plant Vasculature

We investigated how the sucrose surface coating of QD and β-CD affects nanoparticle translocation from the leaf surface into the phloem by confocal fluorescence microscopy imaging (206–233 nm x–y and 2 µm z-axis resolution) (**Figure 3**). The nanoparticles were delivered by foliar application to the adaxial (top) leaf surface in a formulation containing 10 µL of sucQD or QD (200 nM) in buffer (10 mM TES) with 0.1 wt% Silwet L-77, an organosilicone surfactant used to facilitate agrochemical uptake through the plant epidermis. The QDs were imaged by confocal microscopy in the loading area right underneath where the nanoparticles were topically applied on the wheat leaf surface (Figure 3a). After 30 min exposure, unmodified QDs were distributed across the entire leaf within and outside leaf mesophyll cells containing chloroplasts. In contrast, sucQDs were mainly localized in a linear arrangement within leaf areas that were surrounded by leaf mesophyll cells with chloroplasts, indicating uptake into parallel veins of wheat leaves (Figure 3a). To determine the vascular tissue transporting sucQDs, we performed colocalization assays of sucQD with phloem tissue labeled with a fluorescent dye. The 5,6-carboxyfluorescein diacetate (CFDA) is converted into its fluorescent form carboxyfluorescein (CF) when it reacts with cellular esterases after permeation in phloem tissues.[65] This technique is used for live imaging of phloem companion cells and sieve elements in plants.[65] The CF fluorescence emission was imaged within the optical region that does not significantly overlap with the QD fluorescence (< 550 nm) (Figure S6, Supporting Information). The CFDA dye translocated within the leaves and across the vasculature in a similar spatial pattern as sucQD (Figure 3b and Figure S7a,b, Supporting Information). The sucQD fluorescence colocalization with the CF dye (87 ± 5.5%) indicates translocation of sucQDs through the leaf phloem tissue. In contrast, uncoated QDs were not observed to translocate in the leaf vasculature (Figure S7c, Supporting Information). Colocalization experiments of carbon dots with CF dye were not feasible because this fluorescence dye quenches the CD fluorescence emission. To examine the distribution of carbon dots in wheat leaves, Gd-doped CDs applied on the leaf surface were imaged by confocal microscopy and synchrotron X-ray fluorescence (XRF) mapping. In planta confocal fluorescence microscopy images indicated that suc-β-GdCDs were localized in the wheat leaf vasculature 2.2 times higher than the sucrose uncoated β-GdCDs (Figure 3c). We also conducted synchrotron XRF mapping of Gd-ion doped CDs functionalized with β-cyclodextrin and coated with sucrose (suc-β-GdCDs) (Figure S1, Supporting Information). XRF mapping has been previously used in wheat leaf cross sections as a line of evidence of gold nanoparticle loading in the leaf vasculature.[30,66] Gd was chosen to label the CDs for X-ray mapping because of its low background signal in plant tissues, minimal overlap in fluorescence emission energy with elements of interest (Ca, K), and its strong binding affinity with the synthesized CDs.[67] To identify plant cell structures, we used bright-field images of leaf cross sections (Figure 3d) and followed previous studies reporting the use of Ca, and K, X-ray fluorescence emission lines for determining extracellular (apoplastic) and intracellular (symplastic) spaces.[68–70] Ca was used as a main component of the apoplastic middle lamella of plant cell walls while K was associated with the symplastic cell cytoplasm.[71,72] K is an indicator of plant vasculature and a major cation in the phloem sap.[73] The XRF mapping was performed at 0.5 × 0.5 µm resolution on a control wheat leaf without nanoparticles (Figure S8a, Supporting Information) to image the cellular distribution of Ca and K. Both Ca and K have distinguishable fluorescence emission from Gd emission (Figure S8b, Supporting Information), thus these two elements were selected to scan the wheat leaf treated with suc-β-GdCDs (Figure 3e). The XRF map showed the fluorescence emission characteristic of Gd in a selected region containing a leaf vascular bundle. In this region, colocalization analysis of Gd with K (62%) was higher than with Ca (32%), indicating higher delivery inside the vasculature compared to the plant cell wall outer layer. The XRF spectrum for a control leaf without nanoparticles did not exhibit a Gd XRF signal (Figure S8b, Supporting Information). The XRF analysis corroborated that sucrose coating increases the translocation of nanocarriers into the vasculature tissue compared to non-sucrose nanocarrier counterparts.

Nanomaterial physical and chemical properties (i.e., size, charge, amphiphilicity) have been reported to control their translocation in plants.[20,30,43,44,74,75] Smaller nanoparticle DLS size and larger zeta potential have been associated with improved plant cell uptake through cell barriers including the cell wall and plasma membrane. Interestingly, our confocal microscopy and XRF imaging analysis of suc-β-CD and suc-β-GdCD suggest that sucrose moieties enhance vasculature loading of these nanocarriers despite having an increased DLS size or lower zeta potential magnitude than uncoated CD or GdCD. Our findings indicate that surface functionalization with biorecognition molecules is a determining property of the translocation of nanomaterials into the phloem compared to their size and charge over the range of size and charge investigated here. Previous studies reporting QD delivery in plants including the vasculature were demonstrated using non-intact plants in which excised stems were fed with nanoparticle formulations.[59,60] Although these studies provide valuable insights into nanoparticle-plant interactions, they are not practical for agricultural applications or plant biology research that requires in planta technologies. Herein, we demonstrate a scalable and practical method for targeted foliar

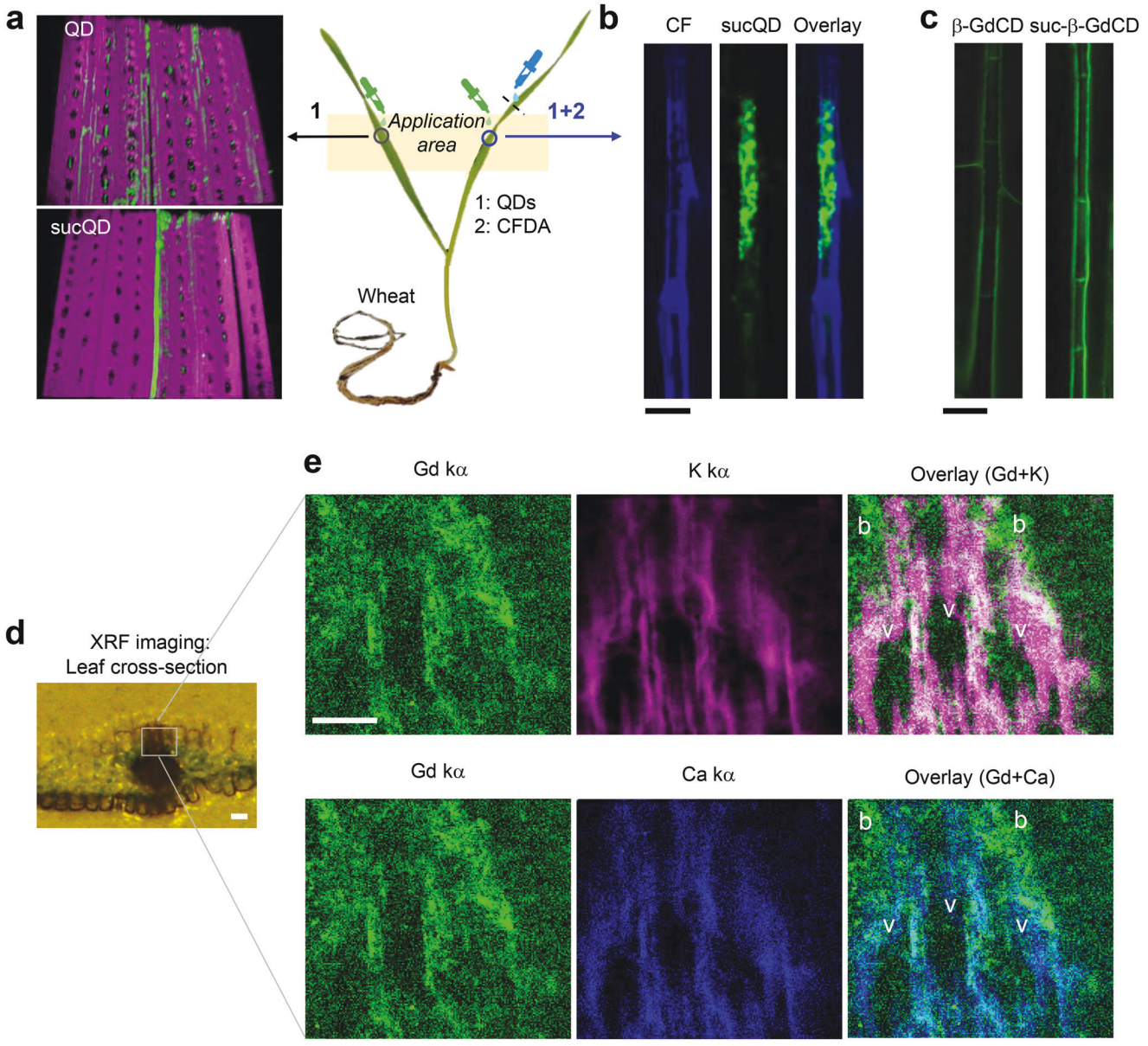

Figure 3. Nanomaterial distribution in leaf vasculature and surrounding mesophyll cells. a) 3D confocal microscopy images of leaves near the QD or sucQD foliar application area in intact live plants show that sucQD (in green) was localized in wheat parallel leaf veins between mesophyll cells containing chloroplasts (in magenta). b) Representative images showing the high colocalization of sucQD with carboxyfluorescein (CF) fluorescent dye that labels phloem cells (in blue). Scale bar = 30 μm. c) In planta confocal fluorescence microscopy images of β-GdCDs and suc-β-GdCDs in wheat leaf vasculature. The suc-β-GdCD were localized in the vasculature 2.2 times higher than the uncoated GdCD. Scale bar = 30 μm. d) Bright-field image of a leaf-dried cross-section exposed to 0.5 μg suc-β-GdCD analyzed by XRF mapping within the selected scanned area. Scale bar = 100 μm. e) XRF maps collected on 5-ID at NSLSII in a selected region of interest in the leaf vascular bundle. The Gd kα XRF images (green) represent suc-β-GdCD and the K kα (magenta) and Ca kα (blue) represent the vasculature tissue. Labels indicate vasculature (v) and bundle sheath (b) tissues in the overlay image. Scale bar = 50 μm.

delivery of CDs with molecular baskets to the phloem of intact live wheat plants, a major field crop with the need for technologies that allow systemic delivery of agrochemicals through the whole plant.[30,76,77] Our approach of coating nanomaterials with sucrose molecules promotes their translocation into the plant vasculature without mechanical aid by facile foliar delivery in planta.

2.3. Translocation of Sucrose Coated Nanoparticles into the Phloem

To investigate the translocation dynamics of nanoparticles in intact live plants, we customized an epifluorescence microscope to detect changes in nanoparticle fluorescence intensity in the leaf vasculature (see Experimental Section, **Figure 4**a). Changes

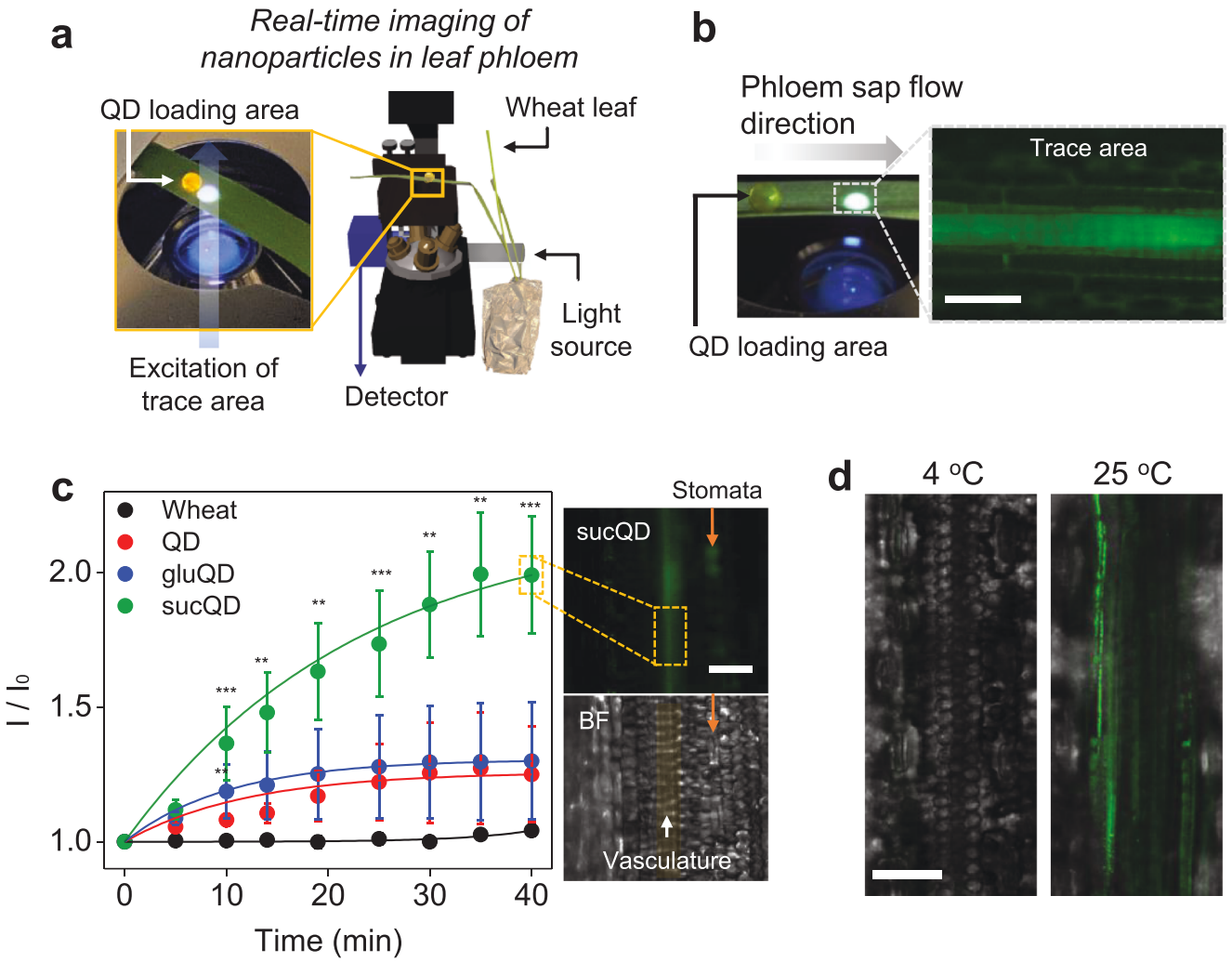

Figure 4. Rapid uptake and translocation of QDs in the phloem is enhanced by nanoparticle sucrose coating. a) Real-time imaging of QD in the phloem of wheat leaves in planta was performed in a customized inverted epifluorescence microscope. A wheat leaf from an intact live plant was mounted on the microscope stage and b) a trace region 10 mm away from the loading area was excited to image QD translocation in the phloem. Scale bar = 100 µm. c) Fluorescence intensity changes in the tracing area indicate rapid loading and translocation of the sucQD in the phloem. The sucQD fluorescence intensity changes were significantly higher than for unmodified QDs and glucose-coated QDs (gluQDs). Epifluorescence image of wheat leaf vasculature after exposure to sucQDs (40 min) indicates sucQD phloem loading and potential pathway of leaf uptake through stomata. Scale bar = 100 µm. One-way ANOVA Dunnett's multiple comparison test (Prism ver. 10, GraphPad), $n = 4$–5, ** $p < 0.01$, *** $p < 0.001$. d) Differences in sucQD translocation in the phloem at 4 and 25 °C indicate a phloem bulk flow-dependent mechanism of nanoparticle loading and translocation into this vascular tissue. $n = 4$. Scale bar = 100 µm. Error bars represent SD.

in QD fluorescence intensity were monitored in real-time downstream of the foliar topical application area (towards the stem) in leaves of intact plants (Figure 4b). The phloem sap in mature intact leaves is transported towards the stem, whereas the xylem sap moves in the opposite direction.[65,78,79] The sucQD fluorescence intensity doubled downstream of the foliar application area during 40 min indicating the nanoparticles are rapidly translocated by the phloem vascular tissue (Figure 4c). In contrast, the unmodified QD fluorescence intensity increased only 1.25 times relative to the initial intensity within the same timeframe. The merged bright-field image of the leaf vasculature with QD fluorescence illustrates the nanoparticle localization in the phloem after 40 min of exposure (Figure 4c and Figure S9, Supporting Information). The rapid translocation of QDs in the leaf vasculature is within the timescale expected for a typical phloem sap velocity of 0.05 to 0.2 mm per second.[80,81] QD fluorescence signals in stomata guard cells on the leaf surface suggest a mechanism of entry via the stomatal pathway into the leaf tissues and the vasculature (Figure 4c). Foliar applied nanoparticles including CDs have been demonstrated to translocate from the leaf surface into mesophyll cells through micron-size stomatal pores.[20,82–85] Silwet L-77 surfactant reduces the water surface tension allowing rapid uptake into leaf stomatal pores and also increases permeability in the epidermal layer through partial removal of the cuticular layer.[20,66] The epifluorescence imaging analysis indicates that sucrose-coated QDs can be rapidly taken up through the leaf epidermis and translocated through the leaf phloem.

To understand the mechanisms guiding sucrose-coated nanomaterials into the phloem, we examined the translocation kinetics of sucQDs and glucose-coated QDs (gluQDs). We hypothesized that the sucrose transporter membrane proteins that facilitate sucrose loading into the phloem increase the binding affinity of sucQDs to the cell membrane of this plant vascular tissue.[86,87] These transporters uptake sucrose and other sugars in phloem cells; however, the specificity to sucrose is much higher than for glucose. The gluQD hydrodynamic size and charge were similar to sucQDs (Table S2, Supporting Information). However, the translocation kinetics of gluQDs was slower and resulted in a 1.25 times increase in fluorescence intensity in the leaf phloem (Figure 4c and Figure S8, Supporting Information), similar to the unmodified QDs indicating that glucose moieties are ineffective at improving QD loading and translocation into the phloem. Although the sucrose coating improves the uptake of sucQDs in the phloem, the translocation of these nanoparticles having a TEM size of 5.0 ± 0.8 nm (n = 16-25) and DLS size of 17.6 ± 1.4 nm (n = 3) (Figure S2 and Table S2, Supporting Information) across sucrose transporters having a maximum size of 0.5 nm [88,89] is not possible. Instead, the sucQDs are likely penetrating the phloem cell membranes by temporary disruptions of the lipid bilayer or by endocytosis. Nanoparticles have been reported to generate an ionic cloud that opens temporary pores in plant lipid membranes.[43,44,90] As an additional line of evidence of sucQD uptake by phloem cells, we compared the effect of temperature on changes in sucQD fluorescence intensity in the leaf vasculature (Figure 4d). Phloem flow has been reported to be inhibited and stopped when chilled to 4 °C by numerous studies,[91–93] an effect that has been attributed to the increase in viscosity, reduced metabolic activity, and other changes in the physical properties of the plant's vascular system.[92–98] Thus we expected to detect sucQDs in the phloem of the leaf trace area away from the loading area at 25 °C but not at 4 °C. Indeed, the sucQD fluorescence emission was observed in the leaf trace area at 25 °C but not when leaves were chilled at 4 °C. The lack of sucQDs in the phloem trace area at low temperatures could be attributed to the reduction in bulk flow of materials including the nanoparticles through the phloem. Overall, these results indicate that sucQDs are preferentially uptaken by the phloem than uncoated QDs and that the nanoparticle uptake by the phloem relies on the bulk flow of the nanomaterials through this vascular tissue.

2.4. Delivery of Chemical Cargoes into the Leaf Vasculature Mediated by Sucrose-Coated Nanocarriers

To assess the potential of targeted nanocarriers for chemical delivery to the plant vasculature, we used a model fluorescent chemical cargo, rhodamine 6G (R6G), that can be loaded in β-cyclodextrins and delivered by nanocarriers (**Figure 5**a). The quenching response of R6G caused by the reaction with β-cyclodextrin through electron transfer,[99] indicates loading of R6G into these molecular baskets (Figure 5b). As the concentration of β-cyclodextrin increases, the R6G fluorescence intensity decreases up to 0.02 μM concentration where there is a saturation of chemical cargo loaded on β-cyclodextrins (Figure 5c). The R6G delivered by CDs functionalized with molecular baskets (β-CDs) without sucrose coating showed weak fluorescence intensity from the vascular tissue. In contrast, when R6G was delivered by suc-β-CD, a higher R6G fluorescence intensity was detected in the vasculature (Figure 5d). When R6G alone was applied to wheat leaves, its fluorescence was primarily observed in the leaf cell walls or membranes but not in the vascular tissue (Figure S10, Supporting Information). We observed a 2.4 times increase in R6G fluorescence when the dye was delivered by suc-β-CD relative to R6G alone. This indicates a significantly improved delivery of the chemical cargoes by sucrose-coated nanocarriers into the leaf vasculature. Our findings demonstrate the effectiveness of a rational design for targeting nanocarriers with chemical cargoes to the plant vasculature using sucrose coatings and the large potential of this approach for improving plant systemic delivery of herbicides or pesticides in nano-enabled agricultural applications.

2.5. Translocation Efficiency of Sucrose-Coated Nanoparticles to Plant Organs through the Plant Vasculature

We quantified both the extent of phloem loading and the distribution of translocated sucQDs compared to unmodified QDs by elemental analysis of Cd in wheat leaves, stems, and roots 24 h after foliar exposure (**Figure 6** and Table S3, Supporting Information). The Cd core within QD allows us to determine the fraction of QD uptake by plant leaves and the fraction transported through the plant by the phloem. The sucQD had an order of magnitude higher overall transport than the unmodified QD, with 13.8 ± 3.4% of sucQDs transported away from the exposed leaf to other plant tissues after 24 h compared to 1.9 ± 0.8% of QDs at the same time. The accumulation of sucQD in roots (8.2 ± 2.7 ng in Cd) was over 6.8 times higher than unmodified QD (1.2 ± 0.9 ng in Cd) 24 h after exposure, indicating a strong enhancement in nanoparticle phloem loading and long-distance transport from leaves to roots mediated by the chemical affinity of sucrose molecules with this vascular tissue. Previous studies have reported nanoparticles (NPs) delivered to the leaf vasculature that translocate away from the exposed leaf, where roots were a significant sink for Au NPs (3, 10, and 50 nm) in wheat plants,[30] TiO_2 and ZnO NPs (25 nm),[100] and polymeric NP carriers (35 nm)[101] in tomato plants. However, most of these phloem-loaded metals and polymer-based NPs lacking biorecognition functionality were transported to young leaves and stems instead of targeting roots.[30,78] The mechanisms for enabling efficient nanoparticle delivery and translocation in the phloem in planta are still under debate because total phloem loading of organic or inorganic nanoparticles is not consistently affected by either nanoparticle size, charge, or hydrophobicity. Our sucrose coating of NP approach enabled targeted NP delivery to roots with ≈70% of phloem-loaded NPs delivered to roots. Sucrose-coated QDs preferential accumulation in the roots relative to uncoated counterparts could be explained by the roots being one of the major sucrose sink organs in plants.[102] Our targeted approach is a significant improvement in delivery to plant root organs compared to a previous study, where less than 30% of phloem-loaded Au NP (10 nm) were transported to wheat roots.[30]

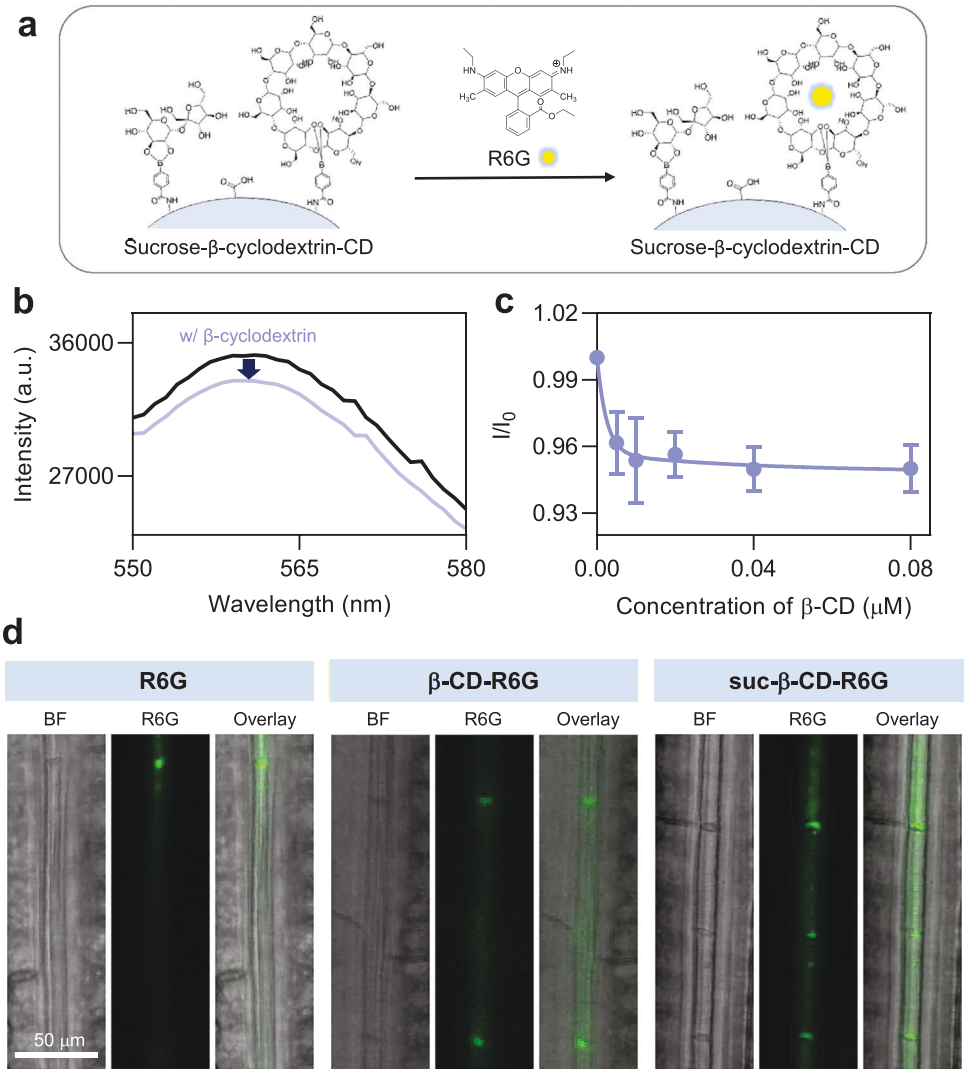

Figure 5. Enhanced delivery of fluorescent chemical cargoes to the leaf vasculature mediated by suc-β-CD a) Schematic of suc-β-CD with molecular basket (β-cyclodextrin) and fluorescent chemical cargo (Rhodamine 6G, R6G). b) Fluorescence spectra of R6G before (black) and after interfacing with 0.05 mM of β-cyclodextrins (purple) (10 mM TES buffer, pH 7.4). c) RG6 fluorescence intensity at different concentrations of β-cyclodextrins ($n = 3$). The data was fitted to a two-phase decay equation. d) Confocal images of wheat leaves indicating enhanced delivery of R6G into the vasculature by nanocarriers coated with sucrose (suc-β-CD) relative to RG6 alone and non-sucrose nanocarrier counterparts (β-CD-RG6). The formulations were suspended in Silwet L-77 (0.1 %) and applied on the adaxial surface of wheat leaves. Error bars represent SD.

2.6. Biocompatibility of Targeted Nanoparticles

The biocompatibility of sucQD and suc-β-CD in wheat leaves was determined by leaf photosynthetic activity and dead cell assays after exposure of wheat leaves to nanomaterials. The sucQD and suc-β-CD did not significantly impact leaf health during the timeframe of the experiments (< 24 h). The leaf CO_2 assimilation rate (A) at different photosynthetically active radiation (PAR) levels of leaves exposed to QD and CD were similar to controls without nanoparticles (**Figure 7**a). Both QD and CD also showed negligible cytotoxic effects in leaves after 24 h of exposure with no significant changes in the percentage of dead leaf mesophyll cells. The percentage of dead cells was determined by staining of nuclei of dead cells with propidium iodide dye (PI) (Figure 7b,c and Figure S11, Supporting Information). The PI dye enters cells with damaged membranes intercalating into double-stranded nucleic acids enabling the quantification of dead cells or damaged cell membranes.[103,104] Together, the biocompatibility assays indicated no toxicity effects of the nanomaterials during our experimental timeframe.

3. Conclusion

Nanoparticle surface coating with biorecognition molecules is a promising approach for the targeted delivery of agrochemical nanocarriers to plant organelles (i.e., chloroplasts),[22,23] cells (i.e., stomata),[24] and vascular tissues (i.e., phloem). Herein, sucQD acting as model traceable nanoparticles for the fundamental understanding of their interactions with plant biosurfaces and suc-β-CD used as nanocarriers for targeted agrochemical delivery

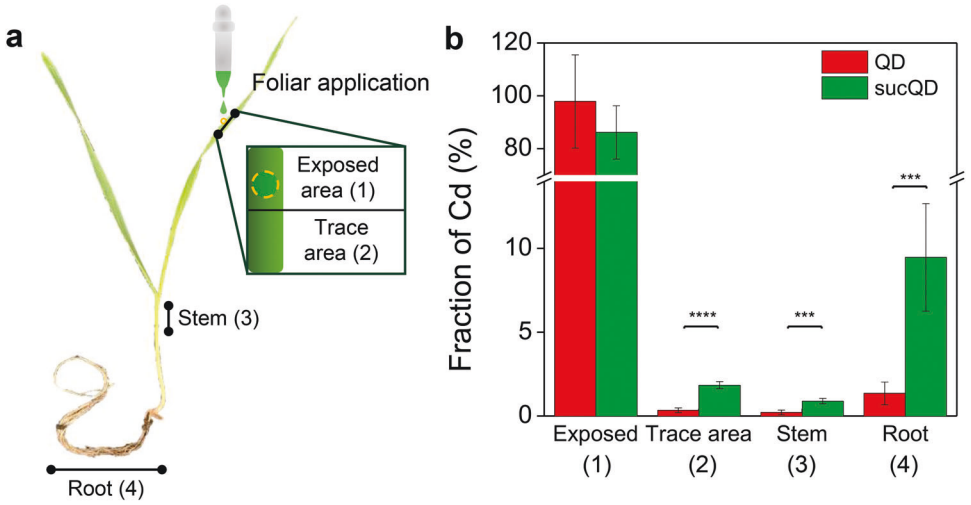

Figure 6. Delivery efficiency of QD from leaves to other plant organs through the phloem. The leaf uptake and translocation of QD and sucQD to wheat plant organs were assessed by ICP-MS analysis of the Cd QD core element. a) Schematic represents sampled areas including exposed and trace leaf areas, stem, and roots. b) The fraction of Cd content detected in wheat plants, after 24 h of nanoparticle exposure, indicates significantly higher translocation of sucQD to all sampled areas including roots compared to unmodified QD. *t*-test (Prism ver. 10, GraphPad), $n = 5$, *** $p < 0.001$, **** $p < 0.0001$. Error bars represent SD.

for agricultural applications allowed us to demonstrate proof of concept of more efficient delivery of sucrose-coated nanoparticles and chemical cargoes to the phloem. The distribution and translocation of sucQD or suc-β-CD in plant leaves were assessed by imaging their fluorescence emission through confocal microscopy in vivo and XRF mapping. The sucrose-coated nanoparticles had high colocalization with the vasculature in leaves, and translocation rates in intact live plants within the time scale and direction (towards the stem) reported for phloem solute transport. The bulk flow-dependent uptake indicates that the sucrose-coated nanomaterials are rapidly taken up through the leaf epidermis and translocated in the phloem. The preferential sucQD loading in phloem vessels over glucose and uncoated QD supports the hypothesis that nanoparticle biorecognition is mediated by the affinity of sucrose moieties with sucrose transporters in phloem cells. Knock-out mutant lines for sucrose transporters with impaired phloem loading are not available in wheat plants but they could be used to test our biorecognition hypothesis in other plant species.[105] Previously, we have demonstrated that carbon dot nanocarriers coated with targeting peptides enhanced the delivery of chemical cargoes to chloroplasts in vivo.[23] Herein, we show that sucrose-coated suc-β-CD nanocarriers significantly enhanced the delivery of chemical cargoes to the phloem. Together these studies highlight that coating

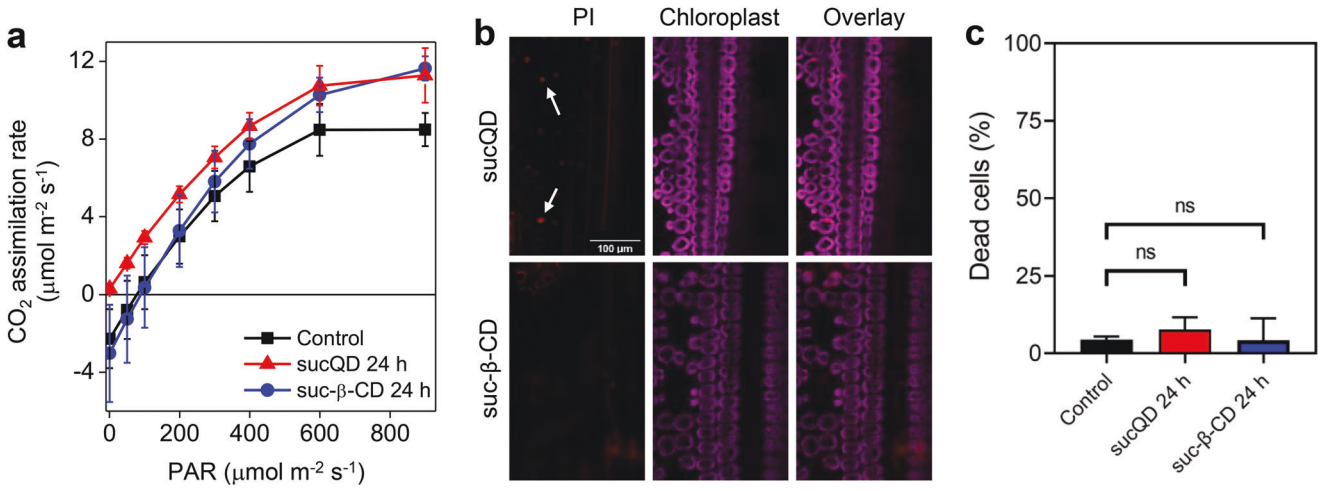

Figure 7. Biocompatibility of sucQD and suc-β-CD with wheat leaves. a) CO_2 assimilation rates at different photosynthetically active radiation (PAR) levels were similar or higher for leaves exposed to sucQD and suc-β-CD relative to controls without nanoparticles ($n = 3$–4). b) Confocal microscopy images of wheat leaves exposed to sucQD and suc-β-CDs for 24 h after being treated with propidium iodide (PI), a fluorescent dye that stains the nuclei of dead cells (white arrows). c) No significant differences in leaf mesophyll cell death were observed between controls without nanoparticles (Silwet-L77 only) and leaves treated with nanomaterials. *t*-test (Prism ver. 10, GraphPad), $n = 4$. Error bars represent SD.

nanocarriers with biomolecules is an effective strategy to improve their delivery and their cargoes to specific tissues or organelles.

Quantitative analysis of sucQD leaf translocation kinetics in planta and long-distance transport analysis were performed by epifluorescence microscopy and ICP-MS of the nanoparticle core elements (Cd), respectively. The sucQDs are delivered by long-distance transport through the phloem from exposed mature leaves to roots was evidenced by a significant increase of Cd in roots. Our targeted approach provides a tool for foliar delivery of nanomaterials with agrochemical cargoes targeted to roots while avoiding interfering interactions with complex and diverse soil matrices. Coating nanoparticles with sucrose enables unprecedented levels of foliar delivery of nanomaterials to roots in intact live plants, a 6.8 times increase in delivery efficiency relative to controls and remarkably 2.4 times higher than previously reported for gold nanoparticle delivery to roots after foliar application.[30] This targeted delivery approach mediated by sucrose coating on the nanomaterial surface was also demonstrated for biocompatible and environmentally friendly nanoparticles such as CD functionalized with molecular baskets able to deliver a wide range of pesticides and herbicides. Future studies would assess the release of targeted nanoparticles from roots into soils that might be expected as plants exude a significant fraction of carbon they fix by photosynthesis[106,107] and nanoparticles have been reported to be exuded from roots into soils.[85] Our carbon dot nanocarrier approach for targeted delivery of agrochemicals could be used to mitigate plant pests such as nematodes that live in the rhizosphere.[108] In addition, applications in the field would require the investigation of interactions with the microbial community at the leaf surface to determine the effect of sucrose-coated nanocarriers on microbial growth.

Technologies for targeted delivery of agrochemicals leading to more sustainable agriculture are required to be scalable, economically viable, and have low environmental footprint.[109] Carbon dot nanocarriers can be synthesized on a large scale through simple bottom-up approaches including thermal synthesis used in this study.[110] In addition, carbon dot nanocarriers are among the most biocompatible nanomaterials made of abundant, economical, and renewable resources including animal and plant derivatives[111] such as urea, citric acid, and saccharides (e.g., sucrose). Biorecognition foliar delivery of nanoparticles and nanocarriers able to carry active ingredients,[23,112] nutrients,[113,114] or DNA/RNA[23] to the phloem can transform current agrochemical delivery technologies into more efficient and sustainable agricultural practices with reduced environmental impact.

4. Experimental Section

Synthesis of Sucrose-Coated QDs (sucQDs): The sucQDs were synthesized from carboxylated QD functionalized with 3-aminophenyl boronic acid (APBA) capped QDs (BA-QD). The carboxylated QDs (QSH-580, Ocean nanotech., USA) were functionalized by 1-ethyl-3-(3-dimethylaminopropyl) carbodiimide (EDC), and N-hydroxysuccinimide (NHS) activated reaction. Briefly, NHS (75 nmol) and EDC/HCl (75 nmol) were added to the 0.5 uM of the carboxylated QDs in TES buffer (10 mM TES buffer, pH 7.4). Then, the mixture was vortexed (750 rpm) for 15 min at ambient temperature. An APBA solution (75 nmol) was added to the activated carboxylated QD solution to generate boronic acid functionalized quantum dots (BA-QDs). The reaction was stirred (750 rpm) for 3 h at room temperature. The excess APBA was removed using a centrifugal filter (30 K amicon filter, Millipore) with ddH_2O and repeated at least five times. To avoid agglomeration during the centrifugation step, a bath sonication step was used to re-suspend the BA-QDs in the centrifugal filter after refilling with ddH_2O. For the synthesis of sucQDs, the BA-QDs were suspended in TES buffer (10 mM TES buffer; pH 10.4), then 15 ul of 5 mM sucrose solution was added to the BA-QD solution and vortexed overnight. The QD reacted with sucrose using a molar ratio of sucrose to QDs of 0.1:1 and obtained a ratio of 0.06:1 for sucrose-coated QD (Figure S3, Supporting Information). Sucrose-coated BA-QDs (sucQDs) were washed using a centrifugal filter (30 K amicon filter, Millipore) in ddH_2O. This step was performed in the same way as the washing step of BA-QDs. The resulting sucQDs were suspended in 10 mM TES (pH 7.5) for experiments in plants.

Synthesis of Sucrose and β-Cyclodextrin-Coated Carbon Dots (suc-β-CDs): The suc-β-CDs were synthesized by coating with β-cyclodextrin and sucrose on the CD core. Core CDs were synthesized by the slight modification of previously reported protocols.[20] The CD cores were synthesized by hydrothermal reactions using citric acid, urea, and ammonium hydroxide. In brief, 1.92 g of citric acid (Fisher, 99.7%) and 2.40 g of urea (Fisher, 99.2%) were dissolved in 2 mL of DI water and 1.35 mL of ammonium hydroxide (Sigma Aldrich, $NH_3 \cdot H_2O$, 30–33%) was added into the mixture. The mixture was reacted at 180 °C for 1.5 h, cooled down to room temperature, and redissolved in DI water. The aggregate was removed by centrifugation at 4500 r.p.m. for 30 min. A solution was further filtered by using a syringe filter (Whatman, pore size, 0.02 µm) to remove large-size particles. Then, the CD core was functionalized by carboxyphenylboronic acid (CBA) capped CD (BA-CD). The NHS (75 nmol) and EDC/HCl (75 nmol) were added to the CD in TES buffer (10 mM TES buffer, pH 7.4). The mixture was vortexed (750 rpm.) for 15 min at ambient temperature. A CBA solution (75 nmol) was added and reacted for 3 h at room temperature. To wash the excess CBA out, a centrifugal filter (3 K amicon filter, Millipore) was used and repeated at least five times. For introducing β-cyclodextrin and sucrose on the sucCD, the BA-CD were dispersed in TES buffer (10 mM TES buffer; pH 10.4), then 10 ul of 5 mM β-cyclodextrin was added and stirred overnight. After the reaction with β-cyclodextrin, the mixture was washed using a centrifugal filter (3 K amicon filter, Millipore) two times. Then 10 µl of 5 mM sucrose was reacted with β-cyclodextrin coated CDs (10 mM TES buffer; pH 10.4). The mixture was washed using a centrifugal filter (3 K amicon filter, Millipore) to remove unbound sucrose. The sucrose to CD molar ratio was not possible to calculate for CD as they do not have a well-defined molecular weight as QD.

Synthesis of Sucrose and β-Cyclodextrin-Coated Gd-Doped Carbon Dots (suc-β-GdCDs): To prepare Gd-doped carbon dots, gadolinium (III) chloride (0.5 g) was dissolved in 6 ml of DI water and then mixed with citric acid (1 g), tritethylenediamine (0.75 ml) in the autoclave reactor. After mixing for 30 min, the reactor was heated at 180 °C for 90 min. The mixture was cooled down on the lab bench, the reaction mixture was centrifuged at 5000 rpm for 30 min to get rid of the aggregates and excess reagents, and the supernatant was then dialyzed (MWCO 1k, Spectrum labs) with 6 L of DI water. The functionalization of GdCD was performed following the same procedure for CD described above.

Characterization of QDs, Carbon Dots, and Gd-Doped Carbon Dots: The absorbance, photoluminescence, hydrodynamic size, zeta potential, and Fourier transform infrared spectroscopy (FT-IR) were measured to characterize their physicochemical properties. Hydrodynamic sizes and zeta potentials were determined in a 10 mM TES buffer (pH 7) in the presence of 0.1 mM NaCl using a Nano-S Malvern Zetasizer. The UV–vis absorption spectra were measured in a UV-2600 Shimadzu spectrophotometer. The concentration of the QDs, CDs, or GdCDs (mg mL^{-1}) was determined using Beer–Lambert's law (Equation (1)), where Abs is absorbance, ϵ is the extinction coefficient, L is the path length, and c is concentration.

$$\mathrm{Abs} = \epsilon \times \mathrm{L} \times \mathrm{c} \quad (1)$$

The absorbance peaks were used for the determination of the concentration at 577 nm for QDs, 400 nm for CDs, and 355 nm for GdCDs. The

extinction coefficient (ϵ) was $2.7 \cdot 10^5$ M^{-1} for QDs, 10.4 mg^{-1} ml for CDs, and 0.18 mg^{-1} ml for GdCDs, with a path length of $L = 10$ mm.

Transmission electron microscopy (TEM) was performed on a Philips FEI Tecnai 12 microscope operated at an accelerating voltage of 120 kV. The TEM samples were prepared by placing one drop of particle solution onto the ultrathin carbon film grid. The surface coatings and functional groups on nanomaterials were characterized by FT-IR (Bruker spectrometer, Alpha I). The FT-IR measurements at each step of the synthesis were taken to analyze functional groups on the nanoparticle surface.

Preparation of Artificial Phloem Sap: Artificial phloem sap was prepared by combining the following chemicals:[115] potassium chloride at 995 mM, calcium chloride at 90 mM, magnesium chloride at 20 mM, sodium nitrate at 5 mM, potassium dihydrogen phosphate at 6 mM, sucrose at 65.9 mM, glucose at 2.5 mM, fructose at 10.3 mM, and citric acid at 28.2 mM.

Plant Growth: Wheat plants (*T. aestivum*) were grown in the F-1200 Plant Growth Chambers (Hipoint, Taiwan) under a light intensity of 200 µmol m^{-2} s^{-1} photosynthetic active radiation, 24 ± 1 and 21 ± 1 °C day/night, 60% relative humidity, and 14/10 h day/night light period. The soil was purchased from Planet Natural (Sunshine Mix #1) and autoclaved before use to avoid unintended effects on plant health and growth by microbial pathogens or other organisms. Each wheat seedling was grown in an individual 2.25-inch square size pot. Plants were watered with tap water once every two days.

Nanoparticle Delivery into Plant Leaves: For fluorescence microscopy, ICP-MS, and X-ray mapping analysis, a solution of 10 uL QD (200 nM) or GdCD (0.1 in 10 mM TES buffer (pH 7.4) with 0.1 wt% Silwet L-77 surfactant was applied topically on the adaxial side of the wheat leaf lamina for 30 min to enable the translocation of nanoparticles across the leaf lamina. The remaining droplets were gently removed by wiping them off with Kimwipes.

Confocal Fluorescence Microscopy of QDs and CDs in Plant Leaves: The QDs were imaged in wheat leaves by using TCS SP5 laser scanning confocal microscope (Leica Microsystems, Germany). Leaves were exposed to QD or CD, as explained above. The leaf disks were collected with a cork borer at the loading area and tracing area (10 mm from the loading area towards the stem) and mounted on a microscopy slide for confocal microscopy imaging of QD or CD. The leaf disks in the microscopy slide were placed inside a chamber made with observation gel (132700, Carolina) filled with 0.3 ml of perfluorodecalin (P9900, Sigma-Aldrich) observation solution for improving confocal imaging. The confocal microscopy settings for QD imaging were as follows: ×20 and ×40 objectives (UAPON-340, 1.15 w); 405 nm laser excitation for QD; *z*-stack section thickness = 2 µm. The PMT detection range was set to 550–600 nm for QD; 700–800 nm for chloroplast autofluorescence; 500–550 nm for CDFA. The confocal microscopy imaging settings for CD imaging were as follows: 355 nm laser excitation; detection range was set to 400–480 nm. All confocal microscopy images were analyzed using FIJI (ImageJ).

Epifluorescence Microscopy of QD Uptake and Translocation into Phloem: To monitor the translocation of sucQDs into the vascular system in real time, fluorescence images were collected by a customized epifluorescence microscopy system. A wheat leaf from an intact live plant was mounted using metal clips on the microscope stage. The QDs were applied on wheat leaves as described above. The roots and soil in the pot were wrapped with aluminum foil to prevent spilling on the microscopy setup. The measurement spot on the abaxial side of the leaf surface was focused 10 mm away from the loading area exposed to sucQD or QD suspension. An arc lamp (U-HGLGPS, Olympus) connected to a band pass excitation filter (400 to 450 nm) was used to excite the QD, and a CCD camera (Retiga R3, Qimaging) for imaging of QD fluorescence emission after a bandpass emission filter (570 to 600 nm). Images were collected using optical cube filters for QD fluorescence emission or chloroplast autofluorescence as follows: For QD, excitation 405 nm, emission detection range was 570–590 nm; for chloroplasts excitation 405 nm, emission detection range was 700–800 nm. The integration time was set at 0.1 s. The collected images were converted to calculate integrated average fluorescence intensity with FIJI (ImageJ).

X-ray Fluorescence Imaging of CD in Plant Leaves: X-ray fluorescence mapping (XRF) images with submicron resolution of dried wheat leaf cross-sections were acquired at Beamline 5-ID at the National Synchrotron Light Source II (NSLS-II) at Brookhaven National Laboratory. Fresh wheat leaves were dosed via drop-deposition with 0.5 µg of sucCDs. The dosed leaves were harvested, cut, submerged in OCT, and immediately flash-frozen in liquid nitrogen. The tissues were cut perpendicular to the leaf vasculature using a cryostat in 50 µm thick slices. Each cross-section was mounted onto a polystyrene cell culture slide sealed between two pieces of Kapton tape. The cross-sections were kept frozen until freeze-dried at −80 °C and 0.133 mbar for 48 h. To acquire XRF images, samples were oriented at 45° to the incoming beam (0.5 × 0.5 µm, 9.5 KeV) and to a four-element Vortex ME3 silicon drift detector. High-resolution XRF maps were collected using a step size of 0.5 µm on fixed tissue with a dwell time of 0.25 s. The spectral fitting was performed using the PyXRF spectral fitting program.

ICP-MS Analysis of QD Distribution in Plant Organs: The plants were digested according to previous protocols with some modifications.[116] All leaf samples were dried at 105 °C for 24 h to remove water. The root samples were air-dried in a fume hood for 15 days to separate adhered soil from root tissue. The dried leaf tissues were weighed and digested overnight at ambient temperature using 0.3 mL of a 2:1 v/v mixture of 70% HNO_3 and 30% H_2O_2. The root samples were digested by 1 mL of a 2:1 70% HNO_3, 30% H_2O_2 mixture. Both samples were heated at 95 °C for 45 min. The samples were then further digested by adding 0.1 or 0.3 mL of 30% HCl into each leaf or root sample, respectively, with another 30 min of heating at 95 °C. Post digestion, the samples were diluted to 5% HNO_3 by MilliQ water and filtered through a 0.45 µm PTFE syringe filter before analysis by ICP-MS (Agilent 7700X). The linearity, precision, and accuracy of the Cd concentration by ICP-MS measurements were assured by calibration (Table S4, Supporting Information) and ICP-MS measurement settings (Table S5, Supporting Information). The percent mass of Cd detected in different plant organs was converted into fractions delivered to each plant organ by the following equation.

$$f(\%) = \frac{m_{Cd\,org}}{m_{Cd\,tot}} \times 100\% \quad (2)$$

where f is the percent of Cd in each plant organ, $m_{Cd\,org}$ is the mass of Cd detected in each plant organ, and $m_{Cd\,tot}$ is the total mass of Cd detected in plants. The percentage of phloem-loaded nanoparticles delivered to the roots was calculated as follows. In sucQD-treated plants, 13.9% of the applied sucQDs were transported outside the exposed zone to other plant organs (after 24 h). Among all the plant organs, 9.5% of the sucQD were detected in plant roots which account for ≈70% of the transported sucQDs.

Leaf Cell Viability Assays: Cell viability of wheat leaves exposed to sucQDs (200 µM) and suc-β-CDs (0.1 mg mL^{-1}) was performed using PI (Propidium iodide, 0.1 mM, plant cell viability assay kit, PA0100, Sigma-Aldrich) as described in the previous report.[46] Briefly, wheat leaves were exposed to buffer control solution (10 mM TES, pH 7.0, 0.1wt% Silwet L-77), sucQDs or suc-β-CDs (in 10 mM TES, pH 7.0, 0.1wt% Silwet L-77). Then, at 3 and 24 h, leaf discs were stained with PI for 30 min. The stained samples were then mounted on microscopy slides for confocal microscopy imaging.[22,90] The PMT detection range was set at 590–640 nm for PI and 690–750 nm for chloroplast autofluorescence under 488 nm excitation. All confocal microscopy images were analyzed using FIJI (ImageJ).

Confocal Imaging of Fluorescent Chemical Cargo Delivery into Plant Cells: A 500 µl of suc-β-CD (0.1 mg ml^{-1}) suspension was incubated for 6 h with 5 µl of rhodamine 6G (0.1 mM) in 10 mM TES buffer (pH 7.4) to load rhodamine 6G on β-cyclodextrins. After incubation, Silwet L-77 was introduced into the solution, resulting in a final concentration of 0.1 wt%. Subsequently, 5 µl of R6G-loaded suc-β-CD was applied on the adaxial side of a wheat leaf. After 1 h treatment, a leaf disc was prepared for confocal imaging as described in methods above. Only R6G or only suc-β-CD in 0.1% Silwet L-77 were applied on leaves as control samples. The confocal microscopy imaging settings were as follows: ×40 wet objective (Carl Zeiss Microsystems, Germany); 355 nm laser excitation for suc-β-CD, 532 nm

laser excitation for rhodamine 6G; 633 nm for chloroplast. The PMT detection range was set at 410–480 nm for suc-β-CD; 540–600 nm for rhodamine 6G; and 680–760 nm for chloroplast autofluorescence.

Statistical Analysis: All data were represented as mean, ± indicates SD, and n = biological replicates or independent nanoparticle sample replicates. Statistical analysis was performed using Prism ver. 10. Statistical comparisons were performed by one-way ANOVA based on post-hoc Dunnett and Tukey tests (two-tailed) or unpaired *t*-test (two-tailed). Statistical significances among experimental groups were denoted by letters and their statistical significance was described by asterisks in captions: $p < 0.05$ (*), $p < 0.01$ (**), $p < 0.001$ (***), and $p < 0.0001$ (****).

Supporting Information

Supporting Information is available from the Wiley Online Library or from the author.

Acknowledgements

This work was supported by the National Science Foundation under Grant No. 1911763 to J.P.G and No. 1911820 to G.V.L. The authors also acknowledge support from BASF CARA award No. 88554036 / RBC026593 to J.P.G. The synchrotron X-ray fluorescence measurements were made on BL 5-ID at NSLSII. The authors thank Andrew Kiss and Juergen Thieme for their assistance in collecting these data.

Conflict of Interest

A pending patent entitled "Compositions and methods for targeted delivery of chemicals and biomolecules to plants and fungi" is based on this work. J.P.G., S.J., and L.M. (University of California, Riverside) are inventors in this patent. Specific aspects of the manuscript covered in the patent disclosure include methods for targeted delivery of nanomaterials to phloem by surface functionalization with sucrose.

Author Contributions

S.J. and J.P.G. conceived and designed the study. S.J. conducted nanoparticle synthesis and characterization, confocal and epifluorescence microscopy, and C.C. performed plant photosynthesis experiments. V.N., K.R., and G.V.L. designed and performed XRF analysis. Y.Z., B.T., and G.V.L. designed and performed ICP-MS analysis. All authors contributed to analyzing datasets and writing the manuscript.

Data Availability Statement

Data supporting the findings of this study are available in the manuscript and Supporting Information or from the corresponding author upon request.

Keywords

active ingredients, environmental nanotechnology, nano-enabled agriculture, phloem, sugars

Received: May 31, 2023
Revised: September 15, 2023
Published online:

[1] United Nations, Department of Economic and Social Affairs, Population Division, World Population prospects: The 2017 Revision, Key Findings and Advance Tables. https://population.un.org/wpp/publications/files/wpp2017_keyfindings.pdf, October, 2017.
[2] G. V. Lowry, A. Avellan, L. M. Gilbertson, *Nat. Nanotechnol.* **2019**, *14*, 517.
[3] C. Dalin, I. Rodríguez-Iturbe, *Environ. Res. Lett.* **2016**, *11*, 035012.
[4] R. S. Defries, T. Rudel, M. Uriarte, M. Hansen, *Nat. Geosci.* **2010**, *3*, 178.
[5] D. Bagchi, F. C. Lau, D. K. Ghosh, BIotechnology in functional foods and nutraceuticals, CRC Press, Florida, USA **2010** p. 197.
[6] A. Sebastian, A. Nangia, M. N. V. Prasad, in *Agrochemicals Detection, Treatment and Remediation* (Ed: M.N.V. Prasad), Butterworth-Heinemann, Amsterdam **2020**, pp. 465–485.
[7] J. Pretty, *Philos. Trans. R. Soc., B* **2008**, *363*, 447.
[8] C. Wilson, C. Tisdell, *Ecol. Econ.* **2001**, *39*, 449.
[9] F. Geiger, J. Bengtsson, F. Berendse, W. W. Weisser, M. Emmerson, M. B. Morales, P. Ceryngier, J. Liira, T. Tscharntke, C. Winqvist, S. Eggers, R. Bommarco, T. Pärt, V. Bretagnolle, M. Plantegenest, L. W. Clement, C. Dennis, C. Palmer, J. J. Oñate, I. Guerrero, V. Hawro, T. Aavik, C. Thies, A. Flohre, S. Hänke, C. Fischer, P. W. Goedhart, P. Inchausti, *Basic Appl. Ecol.* **2010**, *11*, 97.
[10] J. R. Lamichhane, S. Dachbrodt-Saaydeh, P. Kudsk, A. Messéan, *Plant Dis.* **2016**, *100*, 10.
[11] D. Wang, N. B. Saleh, A. Byro, R. Zepp, E. Sahle-Demessie, T. P. Luxton, K. T. Ho, R. M. Burgess, M. Flury, J. C. White, C. Su, *Nat. Nanotechnol.* **2022**, *17*, 347.
[12] A. De, R. Bose, A. Kumar, S. Mozumdar, *Targeted Delivery of Pesticides using Biodegradable Polymeric Nanoparticles*, Springer, New Delhi **2014**.
[13] W. W. Stone, R. J. Gilliom, K. R. Ryberg, *Environ. Sci. Technol.* **2014**, *48*, 11025.
[14] M. C. R. Alavanja, *Rev. Environ. Health* **2009**, *24*, 303.
[15] C. Zhang, Y. Feng, Y.-W. Liu, H.-Q. Chang, Z.-J. Li, J.-M. Xue, *J. Integr. Agric.* **2017**, *16*, 1659.
[16] C. An, C. Sun, N. Li, B. Huang, J. Jiang, Y. Shen, C. Wang, X. Zhao, B. Cui, C. Wang, X. Li, S. Zhan, F. Gao, Z. Zeng, H. Cui, Y. Wang, *J. Nanobiotechnol.* **2022**, *20*, 11.
[17] T. Hofmann, G. V. Lowry, S. Ghoshal, N. Tufenkji, D. Brambilla, J. R. Dutcher, L. M. Gilbertson, J. P. Giraldo, J. M. Kinsella, M. P. Landry, W. Lovell, R. Naccache, M. Paret, J. A. Pedersen, J. M. Unrine, J. C. White, K. J. Wilkinson, *Nat. Food* **2020**, *1*, 416.
[18] S. Husted, F. Minutello, A. Pinna, S. L. Tougaard, P. Møs, P. M. Kopittke, *Trends Plant Sci.* **2023**, *28*, 90.
[19] Q. Liu, B. Chen, Q. Wang, X. Shi, Z. Xiao, J. Lin, X. Fang, *Nano Lett.* **2009**, *9*, 1007.
[20] P. Hu, J. An, M. M. Faulkner, H. Wu, Z. Li, X. Tian, J. P. Giraldo, *ACS Nano* **2020**, *14*, 7970.
[21] R. Nair, S. H. Varghese, B. G. Nair, T. Maekawa, Y. Yoshida, D. S. Kumar, *Plant Sci.* **2010**, *179*, 154.
[22] I. Santana, H. Wu, P. Hu, J. P. Giraldo, *Nat. Commun.* **2020**, *11*, 2045.
[23] I. Santana, S.-J. Jeon, H.-I. Kim, M. R. Islam, C. Castillo, G. F. H. Garcia, G. M. Newkirk, J. P. Giraldo, *ACS Nano* **2022**, *16*, 12156.
[24] E. Spielman-Sun, A. Avellan, G. D. Bland, E. T. Clement, R. V. Tappero, A. S. Acerbo, G. V. Lowry, *Nanoscale* **2020**, *12*, 3630.
[25] J. S. Holt, in *Encyclopedia of Biodiversity*, 2nd ed. (Ed: S.A. Levin), Academic Press, Waltham **2013**, pp. 87–95.
[26] V. Page, U. Feller, *Agronomy* **2015**, *5*, 447.
[27] H. Zhang, C. Zhang, X. Xiang, Q. Zhang, W. Zhao, G. Wei, A. Hu, *Front. Microbiol.* **2022**, *13*, 948171.
[28] K. A. Yadeta, B. P. H. J. Thomma, *Front. Plant Sci.* **2013**, *4*, 97.
[29] Y. Su, V. Ashworth, C. Kim, A. S. Adeleye, P. Rolshausen, C. Roper, J. White, D. Jassby, *Environ. Sci.: Nano* **2019**, *6*, 2311.

[30] A. Avellan, J. Yun, Y. Zhang, E. Spielman-Sun, J. M. Unrine, J. Thieme, J. Li, E. Lombi, G. Bland, G. V. Lowry, *ACS Nano* **2019**, *13*, 5291.
[31] J. Hong, C. Wang, D. C. Wagner, J. L. Gardea-Torresdey, F. He, C. M. Rico, *Environ. Sci.: Nano* **2021**, *8*, 1196.
[32] A. J. E. Van Bel, *Plant, Cell Environ.* **2003**, *26*, 125.
[33] W. J. Lucas, A. Groover, R. Lichtenberger, K. Furuta, S.-R. Yadav, Y. Helariutta, X.-Q. He, H. Fukuda, J. Kang, S. M. Brady, J. W. Patrick, J. Sperry, A. Yoshida, A.-F. López-Millán, M. A. Grusak, P. Kachroo, *J. Integr. Plant Biol.* **2013**, *55*, 294.
[34] S. Dinant, R. Lemoine, *C. R. Biol.* **2010**, *333*, 307.
[35] K. J. Oparka, S. S. Cruz, *Annu. Rev. Plant Physiol. Plant Mol. Biol.* **2000**, *51*, 323.
[36] K. J. Oparka, R. Turgeon, *Plant Cell* **1999**, *11*, 739.
[37] M. Knoblauch, K. Oparka, *Plant J.* **2012**, *70*, 147.
[38] R. Viola, A. G. Roberts, S. Haupt, S. Gazzani, R. D. Hancock, N. Marmiroli, G. C. Machray, K. J. Oparka, *Plant Cell* **2001**, *13*, 385.
[39] A. G. Roberts, S. S. Cruz, I. M. Roberts, D. A. M. Prior, R. Turgeon, K. J. Oparka, *Plant Cell* **1997**, *9*, 1381.
[40] M. J. Gravato-Nobre, M. A. McClure, L. Dolan, G. Calder, K. G. Davies, B. Mulligan, K. Evans, N. von Mende, *J. Nematol.* **1999**, *31*, 212.
[41] J. S. Kim, G. Daniel, *Trees* **2017**, *31*, 1335.
[42] N. D. DeWitt, M. R. Sussman, *Plant Cell* **1995**, *7*, 2053.
[43] T. T. S. Lew, M. H. Wong, S.-Y. Kwak, R. Sinclair, V. B. Koman, M. S. Strano, *Small* **2018**, *14*, 1802086.
[44] M. H. Wong, R. P. Misra, J. P. Giraldo, S.-Y. Kwak, Y. Son, M. P. Landry, J. W. Swan, D. Blankschtein, M. S. Strano, *Nano Lett.* **2016**, *16*, 1161.
[45] D. A. Navarro, M. A. Bisson, D. S. Aga, *J. Hazard. Mater.* **2012**, *211–212*, 427.
[46] J. Li, H. Wu, I. Santana, M. Fahlgren, J. P. Giraldo, *ACS Appl. Mater. Interfaces* **2018**, *10*, 28279.
[47] Y. Koo, J. Wang, Q. Zhang, H. Zhu, E. W. Chehab, V. L. Colvin, P. J. J. Alvarez, J. Braam, *Environ. Sci. Technol.* **2015**, *49*, 626.
[48] R. Hardman, *Environ. Health Perspect.* **2006**, *114*, 165.
[49] S. Saha, A. Roy, K. Roy, M. N. Roy, *Sci. Rep.* **2016**, *6*, 35764.
[50] J. Szejtli, *Chem. Rev.* **1998**, *98*, 1743.
[51] D. Bouzas-Ramos, J. Cigales Canga, J. C. Mayo, R. M. Sainz, J. Ruiz Encinar, J. M. Costa-Fernandez, *Adv. Funct. Mater.* **2019**, *29*, 1903884.
[52] J. Liu, R. Li, B. Yang, *ACS Cent. Sci.* **2020**, *6*, 2179.
[53] B. K. John, T. Abraham, B. Mathew, *J. Fluoresc.* **2022**, *32*, 449.
[54] Y. Li, X. Xu, Y. Wu, J. Zhuang, X. Zhang, H. Zhang, B. Lei, C. Hu, Y. Liu, *Mater. Chem. Front.* **2020**, *4*, 437.
[55] X. Shi, W. Wei, Z. Fu, W. Gao, C. Zhang, Q. Zhao, F. Deng, X. Lu, *Talanta* **2019**, *194*, 809.
[56] A. Wang, F. Kang, Z. Wang, Q. Shao, Z. Li, G. Zhu, J. Lu, Y. Y. Li, *Adv. Sustainable Syst.* **2019**, *3*, 1800132.
[57] H. Li, J. Huang, F. Lu, Y. Liu, Y. Song, Y. Sun, J. Zhong, H. Huang, Y. Wang, S. Li, Y. Lifshitz, S.-T. Lee, Z. Kang, *ACS Appl. Bio Mater.* **2018**, *1*, 663.
[58] H. Li, C. Sun, R. Vijayaraghavan, F. Zhou, X. Zhang, D. R. Macfarlane, *Carbon* **2016**, *104*, 33.
[59] N. Al-Salim, E. Barraclough, E. Burgess, B. Clothier, M. Deurer, S. Green, L. Malone, G. Weir, *Sci. Total Environ.* **2011**, *409*, 3237.
[60] M. Alimohammadi, Y. Xu, D. Wang, A. S. Biris, M. V. Khodakovskaya, *Nanotechnology* **2011**, *22*, 295101.
[61] T. Ducic, I. Milenkovic, D. Mutavdzic, M. Nikolic, M. V. M. De Yuso, Z. Vucinic, M. Algarra, K. Radotic, *Colloids Surf., B* **2021**, *204*, 111828.
[62] C. Yu, T. Xuan, Y. Chen, Z. Zhao, X. Liu, G. Lian, H. Li, *J. Alloys Compd.* **2016**, *688*, 611.
[63] L. Wang, W. Zhou, D. Yang, H. Zhe, S. Mei, J. Yuan, W. Zhang, H. Li, H. Fan, F. Xie, R. Guo, *Anal. Methods* **2021**, *13*, 2442.
[64] Y. Xu, X.-H. Jia, X.-B. Yin, X.-W. He, Y.-K. Zhang, *Anal. Chem.* **2014**, *86*, 12122.
[65] T. Cayla, B. Batailler, R. Le Hir, F. Revers, J. A. Anstead, G. A. Thompson, O. Grandjean, S. Dinant, *PLoS One* **2015**, *10*, 0118122.
[66] A. Avellan, J. Yun, B. P. Morais, E. T. Clement, S. M. Rodrigues, G. V. Lowry, *Environ. Sci. Technol.* **2021**, *55*, 13417.
[67] Y. Pan, J. Yang, Y. Fang, J. Zheng, R. Song, C. Yi, *J. Mater. Chem. B* **2017**, *5*, 92.
[68] S. Majumdar, J. . Peralta-Videa, H. Castillo-Michel, J. Hong, C. M. Rico, J. L. Gardea-Torresdey, *Anal. Chim. Acta* **2012**, *755*, 1.
[69] E. Spielman-Sun, A. Avellan, G. D. Bland, R. V. Tappero, A. S. Acerbo, J. M. Unrine, J. P. Giraldo, G. V. Lowry, *Environ. Sci.: Nano* **2019**, *6*, 2508.
[70] M. Tsednee, M. Castruita, P. A. Salomé, A. Sharma, B. E. Lewis, S. R. Schmollinger, D. Strenkert, K. Holbrook, M. S. Otegui, K. Khatua, S. Das, A. Datta, S.i Chen, C. Ramon, M. Ralle, P. K. Weber, T. L. Stemmler, J. Pett-Ridge, B. M. Hoffman, S. S. Merchant, *J. Biol. Chem.* **2019**, *294*, 17626.
[71] R. C. Leegood, T. D. Sharkey, S. von Caemmerer, *Photosynthesis: Physiology and Metabolism*, Springer, Germany, **2006**, p. 590.
[72] L. Taiz, I. M. Møller, A. Murphy, E. Zeiger, *Plant Physiology and Development*, Oxford University Press, New York **2022**.
[73] P. Gajdanowicz, E. Michard, M. Sandmann, M. Rocha, L. G. G. Corrêa, S. J. Ramírez-Aguilar, J. L. Gomez-Porras, W. González, J.-B. Thibaud, J. T. Van Dongen, I. Dreyer, *Proc. Natl. Acad. Sci. U. S. A.* **2011**, *108*, 864.
[74] S.-Y. Kwak, T. T. S. Lew, C. J. Sweeney, V. B. Koman, M. H. Wong, K. Bohmert-Tatarev, K. D. Snell, J. S. Seo, N.-H. Chua, M. S. Strano, *Nat. Nanotechnol.* **2019**, *14*, 447.
[75] G. S. Demirer, H. Zhang, J. L. Matos, N. S. Goh, F. J. Cunningham, Y. Sung, R. Chang, A. J. Aditham, L. Chio, M.-J.e Cho, B. Staskawicz, M. P. Landry, *Nat. Nanotechnol.* **2019**, *14*, 456.
[76] C. L. Doolette, T. L. Read, C. Li, K. G. Scheckel, E. Donner, P. M. Kopittke, J. K. Schjoerring, E. Lombi, *J. Exp. Bot.* **2018**, *69*, 4469.
[77] W Zhang, , Proceedings of the International Academy of Ecology and EnvironmentalSciences **2018**, *8*, 1.
[78] Y. Zhang, L. Fu, S. Li, J. Yan, M. Sun, J. P. Giraldo, K. Matyjaszewski, R. D. Tilton, G. V. Lowry, *Environ. Sci. Technol.* **2021**, *55*, 10758.
[79] M. R. Thorpe, A. P. Ferrieri, M. M. Herth, R. A. Ferrieri, *Planta* **2007**, *226*, 541.
[80] S. Payvandi, K. R. Daly, K. C. Zygalakis, T. Roose, *Bull. Math. Biol.* **2014**, *76*, 2834.
[81] J. A. Savage, M. A. Zwieniecki, N. M. Holbrook, *Plant Physiol.* **2013**, *163*, 1409.
[82] N. Ha, E. Seo, S. Kim, S. J. Lee, *Sci. Rep.* **2021**, *11*, 11556.
[83] R. Raliya, C. Franke, S. Chavalmane, R. Nair, N. Reed, P. Biswas, *Front. Plant Sci.* **2016**, *7*, 1288.
[84] K. Banerjee, P. Pramanik, A. Maity, D. C. Joshi, S. H. Wani, P. Krishnan, in *Advances in Phytonanotechnology: From Synthesis to Application* (Eds: M. Ghorbanpour, S. H. Wani), Academic Press, London **2019**, pp. 123–152.
[85] A. Avellan, J. Yun, Y. Zhang, E. Spielman-Sun, J. M. Unrine, J. Thieme, J. Li, E. Lombi, G. Bland, G. V. Lowry, *ACS Nano* **2019**, *13*, 5291.
[86] A. Reinders, *Front. Plant Sci.* **2012**, *3*, 22.
[87] Y. Sun, J. M. Ward, *BMC Biochem.* **2012**, *13*, 26.
[88] S. Lalonde, E. Boles, H. Hellmann, L. Barker, J. W. Patrick, W. B. Frommer, J. M. Ward, *Plant Cell* **1999**, *11*, 707.
[89] R. J. Milne, J. M. Perroux, A. L. Rae, A. Reinders, J. M. Ward, C. E. Offler, J. W. Patrick, C. P. L. Grof, *Plant Physiol.* **2017**, *173*, 1330.
[90] H. Wu, N. Tito, J. P. Giraldo, *ACS Nano* **2017**, *11*, 11283.
[91] I. F. Wardlaw, D. Bagnall, *Plant Physiol.* **1981**, *68*, 411.
[92] A. A. Schrier, G. Hoffmann-Thoma, A. J. E. Van Bel, *Funct. Plant Biol.* **2000**, *27*, 769.
[93] R. F. Evert, *Esau's Plant Anatomy: Meristems, Cells, and Tissues of the Plant Body: Their Structure, Function, and Development*, John Wiley & Sons, Hoboken, NJ **2006**.

[94] R. Crang, S. Lyons-Sobaski, R. Wise, *Plant Anatomy: A Concept-Based Approach to the Structure of Seed Plants*, Springer, Cham, Switzerland **2018**.
[95] P. Laine, J. Bigot, A. Ourry, J. Boucaud, *New Phytol.* **1994**, *127*, 675.
[96] J. Hao, F. Gu, J. Zhu, S. Lu, Y. Liu, Y. Li, W. Chen, L. Wang, S. Fan, C. J. Xian, *PLoS One* **2016**, *11*, 0160909.
[97] J. A. Savage, I. Chuine, *New Phytol.* **2021**, *230*, 1700.
[98] M. R. Dumlao, A. Darehshouri, C. M. Cohu, O. Muller, J. Mathias, W. W. Adams, B. Demmig-Adams, *Photosynth. Res.* **2012**, *113*, 181.
[99] J. Liu, G. Liu, W. Liu, Y. Wang, M. Xu, B. Wang, *Mikrochim. Acta* **2016**, *183*, 1161.
[100] R. Raliya, R. Nair, S. Chavalmane, W.-N. Wang, P. Biswas, *Metallomics* **2015**, *7*, 1584.
[101] Y. Zhang, L. Fu, S.-J. Jeon, J. Yan, J. P. Giraldo, K. Matyjaszewski, R. D. Tilton, G. V. Lowry, *ACS Nano* **2022**, *16*, 4467.
[102] N. Hennion, M. Durand, C. Vriet, J. Doidy, L. Maurousset, R. Lemoine, N. Pourtau, *Physiol. Plant.* **2019**, *165*, 44.
[103] K. Jones, D. W. Kim, J. S. Park, C. H. Khang, *BMC Plant Biol.* **2016**, *16*, 69.
[104] H. Zhao, J. Oczos, P. Janowski, D. Trembecka, J. Dobrucki, Z. Darzynkiewicz, D. Wlodkowic, *Cytometry A* **2010**, *77*, 399.
[105] M. Bezrutczyk, T. Hartwig, M. Horschman, S. N. Char, J. Yang, B. Yang, W. B. Frommer, D. Sosso, *New Phytol.* **2018**, *218*, 594.
[106] S. Haldar, S. Sengupta, *Open Microbiol. J.* **2015**, *9*, 1.
[107] C. E. Prescott, S. J. Grayston, H.-S. Helmisaari, E. Kastovská, C. Körner, H. Lambers, I. C. Meier, P. Millard, I. Ostonen, *Trends Ecol. Evol.* **2020**, *35*, 1110.
[108] A. A. Caparco, I. González-Gamboa, S. S. Hays, J. K. Pokorski, N. F. Steinmetz, *Nano Lett.* **2023**, *23*, 5785.
[109] M. Kah, R. S. Kookana, A. Gogos, T. D. Bucheli, *Nat. Nanotechnol.* **2018**, *13*, 677.
[110] L. Đordevic, F. Arcudi, M. Cacioppo, M. Prato, *Nat. Nanotechnol.* **2022**, *17*, 112.
[111] V. Sharma, P. Tiwari, S. M. Mobin, *J. Mater. Chem. B* **2017**, *5*, 8904.
[112] H. I. Hussain, Z. Yi, J. E. Rookes, L. X. Kong, D. M. Cahill, *J. Nanopart. Res.* **2013**, *15*, 1676.
[113] J. Borgatta, C. Ma, N. Hudson-Smith, W. Elmer, C. D. Plaza Pérez, R. De La Torre-Roche, N. Zuverza-Mena, C. L. Haynes, J. C. White, R. J. Hamers, *ACS Sustainable Chem. Eng.* **2018**, *6*, 14847.
[114] C. Ma, J. Borgatta, B. G. Hudson, A. A. Tamijani, R. De La Torre-Roche, N. Zuverza-Mena, Y. Shen, W. Elmer, B. Xing, S. E. Mason, R. J. Hamers, J. C. White, *Nat. Nanotechnol.* **2020**, *15*, 1033.
[115] Y. Su, V. E. T. M. Ashworth, N. K. Geitner, M. R. Wiesner, N. Ginnan, P. Rolshausen, C. Roper, D. Jassby, *ACS Nano* **2020**, *14*, 2966.
[116] Y. Zhang, J. Yan, A. Avellan, X. Gao, K. Matyjaszewski, R. D. Tilton, G. V. Lowry, *ACS Nano* **2020**, *14*, 10954.

